SSRG International Journal of Electrical and Electronics Engineering
ISSN: 2348-8379/ https://doi.org/10.14445/23488379/IJEEE-V11I4P113

Volume 11 Issue 4, 118-129, April 2024

Original Article

Adaptive Neuro-Fuzzy Control of a Single-Sided AFPMSM Motor for Electric Vehicle Applications

Vo Thanh Ha[1], Nguyen Van Hai[2]

[1,2]*Faculty of Electrical and Electronic Engineering, University of Transport and Communications, Hanoi, Vietnam*

[2]*Corresponding Author : haiktdt@utc.edu.vn*

Received: 09 February 2024 Revised: 09 March 2024 Accepted: 08 April 2024 Published: 30 April 2024

Abstract - *This study will present the torque control design of an in-wheel single-sided AFPMSM motor utilizing Adaptive Neuro-Fuzzy (ANFIS) techniques powered by a two-level inverter. The neuro-fuzzy intelligent controller will be constructed using a neural network-based feature set and a fuzzy system. The neural network will process the dataset concerning the stator current error (e) and error integral (Δe). This dataset will be fed into the fuzzy logic approach to establish control rules. The ANFIS controller will undergo training and testing stages. An evaluation will compare the efficiency of the FLC, ANFIS torque, and PI controllers. The results of MATLAB/SIMULINK simulations illustrate that the proposed ANFIS torque controllers deliver precise control. The MATLAB/SIMULINK simulation results demonstrate that the ANFIS torque controllers exhibit greater precision than the PI controller. This study underscores the efficacy of employing the adaptive neuro-fuzzy technique, particularly with a two-level inverter, to ensure precise torque control for in-wheel single-sided AFPMSM motors. The amalgamation of neuro-fuzzy intelligent control, neural network-based feature sets, and fuzzy systems demonstrate promise in enhancing motor control design.*

Keywords - *AFPMSM, FLC ANFIS, PID, Electrical vehicle, FOC.*

1. Introduction

Electric vehicles are a revolutionary development in modern transportation, offering advantages over traditional internal combustion engine vehicles. By eliminating complex transmissions and reducing pollution, electric vehicles are not only environmentally friendly but also efficient. These vehicles typically use an in-wheel distributed electric drive system with multiple motors to provide traction to the front or rear wheels, resulting in various drive configurations. The electric powertrain optimizes energy distribution between the wheels, enhancing driving performance by improving energy utilization, transmission efficiency, range, braking, heat dissipation, and ease of installation and maintenance.

The Axial Flux Permanent Magnet Synchronous Motor (AFPMSM) is commonly used in electric buses and in-wheel motor driving systems for tanks. Its lightweight rotor, strong vibration resistance, and long service life contribute to the engine's reliability and safety. However, managing multiple motors in each vehicle can be complex. In addition, the in-wheel motor system increases costs and requires advanced control technologies such as power balancing, electronic differential, and energy recovery. These systems must have compact dimensions, low weight, modest torque, high efficiency, substantial overload capacity, and a wide speed range. Researchers are exploring ways to effectively control the traction and torque of the AFPMSM motor in-wheel to ensure optimal performance. Direct Torque Control (DTC) and Field-Oriented Control (FOC) are used to regulate torque and speed controllers.

Moreover, these controllers utilize various linear and nonlinear control techniques, such as PI, LQR, deadbeat, sliding control, flatness, fuzzy, or hybrid controllers like fuzzy-neural and fuzzy-sliding mode control. This research specifically focuses on evaluating different torque and speed regulation approaches in AFPMSM motors under constant load torque or specific motor characteristics. While the torque response may show slight pulsations, the speed response consistently and accurately tracks the desired speed, as referenced in [15, 16].

Studies indicate that exploring intelligent control methods could improve the torque of an AFPMSM motor integrated into an electric car's in-wheel system, considering the required torque component based on the vehicle's physical attributes. Factors such as brake pedals, accelerator pedals, road incline effects, and air resistance play a crucial role in boosting the efficiency and performance of electric vehicles.

This study presents the control design of an in-wheel AFPMSM motor with one stator and one rotor, employing

fuzzy logic and a neuro-fuzzy controller for an electric vehicle. The FLC controller builds the Surgeon ambiguous inference file using two input vectors: the stator current error and the derivative of the stator error. Input variables comprise five membership functions: Negative Ample (NB), Negative Small (NS), Equal Zero (ZE), Positive Small (PS), and Positive Ample (PB). The fuzzy logic controller utilizes a 5x5 matrix to ensure the output stator voltage meets specified requirements [9, 17, 18].

On the other hand, the ANFIS controller is employed for the neural network-based feature set and the fuzzy system. A structured, forward-looking network characterizes the neural network, with the training process involving backpropagation. Training data is utilized to minimize network error during backpropagation.

A suitable control model can be developed accordingly. The proposed fuzzy inference system model is based on the Sugeno model, incorporating rules. The concept encompasses three stages: fuzzification, rule-based decision-making, and defuzzification.

The neural network in this hybrid system generates the dataset based on the discrepancy between the natural line and its integral. This dataset is fed into the fuzzy system, creating control rules [19-21]. The training and testing phases impact the ANFIS controller. A comparison is drawn between the FLC, ANFIS torque controllers, and PI controllers.

The paper comprises six main sections. Section 2 introduces the state model of the electric vehicle traction transmission system. Section 3 details the development of a torque controller using Fuzzy Logic Control (FLC) and Adaptive Neuro-Fuzzy Inference System (ANFIS) methods guided by mathematical formulas. Simulation results and an assessment of the proposed controller's current, speed, and torque responses compared to the PI controller are presented in Section 4 to demonstrate the theory's validity. The paper concludes by discussing the study findings and suggestions for improving torque response through basic controller design theory and practical application.

2. Mathematical Model of AFPMSM Drive System

2.1. Mathematical Model of an AFPMSM Motor

The single-sided AFPMSM means that the AFPMSM motor has one stator and one rotor. Therefore, the AFPMSM can use the Permanent Magnet Synchronous Motor model (PMSM) [13]. However, the AFPMSM mathematical model has differences in stator winding parameter values, and the motor Back-EMF generated by a permanent magnet and an excitation coil does not differ. The stator voltage equation in the d-q reference system is calculated according to Equations 1 and 2. The application method is written as follows:

$$\begin{bmatrix} u_{sd} \\ u_{sq} \end{bmatrix} = \begin{bmatrix} R_{sq} + \frac{dL_{sq}}{dt} & \omega_m L_{sd} \\ -\omega_m L_{sd} & R_{sd} + \frac{dL_{sd}}{dt} \end{bmatrix} \begin{bmatrix} i_{sd} \\ i_{sq} \end{bmatrix} + \begin{bmatrix} \omega_m \lambda_m \\ 0 \end{bmatrix} \quad (1)$$

The moment equation is determined as follows:

$$T_m = \frac{3}{2}\frac{P}{2}(L_{sd} i_{sq} + \lambda_m) i_{sq} - (L_{sq} i_{sq}) \quad (2)$$

Since the information is a constant, the proportional description is convenient for the flow stator axis of rotation q. The electromagnetic module submission is selected by the Equation 3:

$$T_m = \frac{3}{4} P \lambda_m i_{sq} \quad (3)$$

2.2. Mathematica Model of Electric Cars

Drive wheel model as Equation 4:

$$\begin{cases} v_{wh} = \omega_{wh} R_{wh} \\ T_{wh} = T_L = F_t R_{wh} \end{cases} \quad (4)$$

When the wheel presses against the road surface with force N and is driven by a torque of T_{wh} the vehicle will exert a force on the road surface F. Correspondingly, the road surface acts against the vehicle with a force of the same value in the opposite direction F_t . In this case, then F_t is the force of friction and is the useful force component that creates the movement of the vehicle at speed V_x

$$F_t = m_v . g . \mu \quad (5)$$

Applying Newton's second law to the external force components acting on the vehicle body, we have the equation Equation 6:

$$m_v \frac{dv_{ev}}{dt} = F_t - F_{aero} - F_{roll} - m_v . g . \sin\alpha \quad (6)$$

Air resistance

$$F_{aero} = \frac{\rho C_d A_F}{2} (v_{ev} + v_{win})^2 \quad (7)$$

In some cases or simulations, we can consider wind speed $v_{wind} = 0$. Rolling resistance exists in case the tire is under-inflated:

$$F_{roll} = f_r F_{zY} \quad (8)$$

$$F_{zY} = m_v g \cos\alpha \quad (9)$$

3. Design of Torque Controller

3.1. Design of PI Torque Controller

Developing torque regulators for the AFPMSM engine is vital for top-notch applications. Crafting current regulators for

the AFPMSM closely resembles those for asynchronous motor systems. To devise a torque regulator for the AFPMSM, a profound understanding of the interplay between the motor, inverter, and the current regulator is indispensable. Assuming the inverter possesses a K_r gain and a T_r time constant-equivalent to half the pulse width modulation carrier frequency period-the current control loop's targeted performance aligns with a first-order hysteresis system.

$$\frac{i_{sd}}{i_{sd}^*} = \frac{K_i}{1+ sT_i} \tag{10}$$

Stator current loop is shown:

$$\frac{i_{sq}}{i_{sq}^*} = \frac{K_a K_t (1+T_m s}{H_c K_a K_r (1+ sT_m)+(1+ sT_r)[K_a K_b+(1+ sT_a)(1+ sT_m)]} \tag{11}$$

The following approximations are valid near the vicinity of the crossover frequency.

$$(1 + sT_a)(1 + sT_r) \cong 1 + s((T_a + T_r) \tag{12}$$

$$\cong 1 + s((T_a + T_r)$$

The current transfer function is rewritten as follows:

$$\frac{i_{sq}}{i_{sq}^*} = \frac{(K_a K_t T_m)s}{K_a K_b+(T_m+K_a K_t T_m H_c)s+(T_m T_{af})s^2} \tag{13}$$

The stator current loop is given by:

$$\frac{i_{sq}}{i_{sq}^*} \cong \frac{K_i s}{(1+sT_i)} \tag{14}$$

Where: $K_i = \frac{T_m K_r}{T_2 K_b}$; $T_i = T_1$

3.2. FLC Torque Controller Design

By calculating the necessary voltage u_{sd}, u_{sq}, the fuzzy logic controller controls the system so that the difference between current i_{sd} and i_{sq} is as tiny as possible. The exactly planned isd and isq stator currents are used here to regulate the motor's torque control current. This paper will outline the modern controller design for the i_{sd}.

The control strategy for an AFPMSM motor, one stator, and one rotor utilizing an FLC controller for electric car in-wheels is presented in this work. The stator current error and the derivative of the stator error are used as the two input vectors in this controller to build the Surgeon ambiguous inference file. Five membership functions are included in these input variables: Positive Big (PB), Positive Small (PS), Equal Zero (ZE), and Negative Big (NB), Negative Small (NS). As seen in Table 1 and Figure 1, the fuzzy logic controller is constructed using a 5x5 matrix.

The fuzzy logic control rule consists of 25 rules, which are implemented as follows:

- If (input 1 is NB) and (input 2 is NB), then (output is NB)
- If (input 1 is NB) and (input 2 is NS), then (output is NB)
- If (input 1 is NB) and (input 2 is ZE), then (output is NB)
- If (input 1 is NB) and (input 2 is PS), then (output is NS)
- If (input 1 is NB) and (input 2 is PB), then (output is ZE)
- ……
- If (input 1 is PS) and (input 2 is PB), then (output is PB)

Table 1. Matrix of controller

Input 2 (Δe)/Input 1 (e)	NB	NS	ZE	PS	PB
NB	NB	NB	NB	NS	ZE
NS	NB	NB	NS	ZE	PS
ZE	NS	NS	ZE	PS	PB
PS	ZE	ZE	PS	PB	PB
PB	ZE	PS	PB	PB	PB

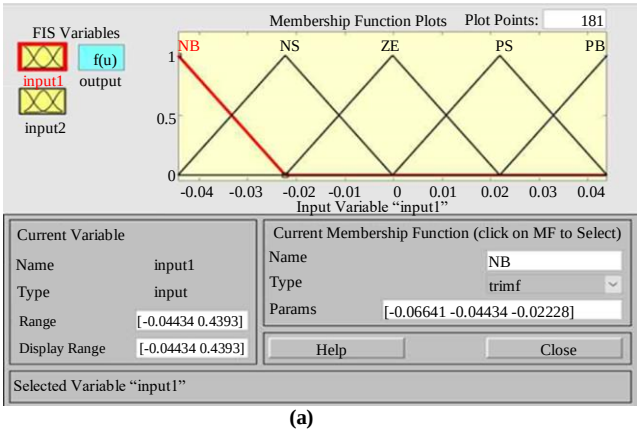

(a)

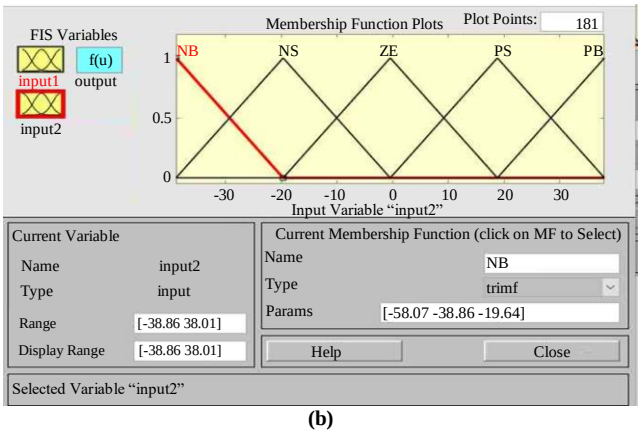

(b)

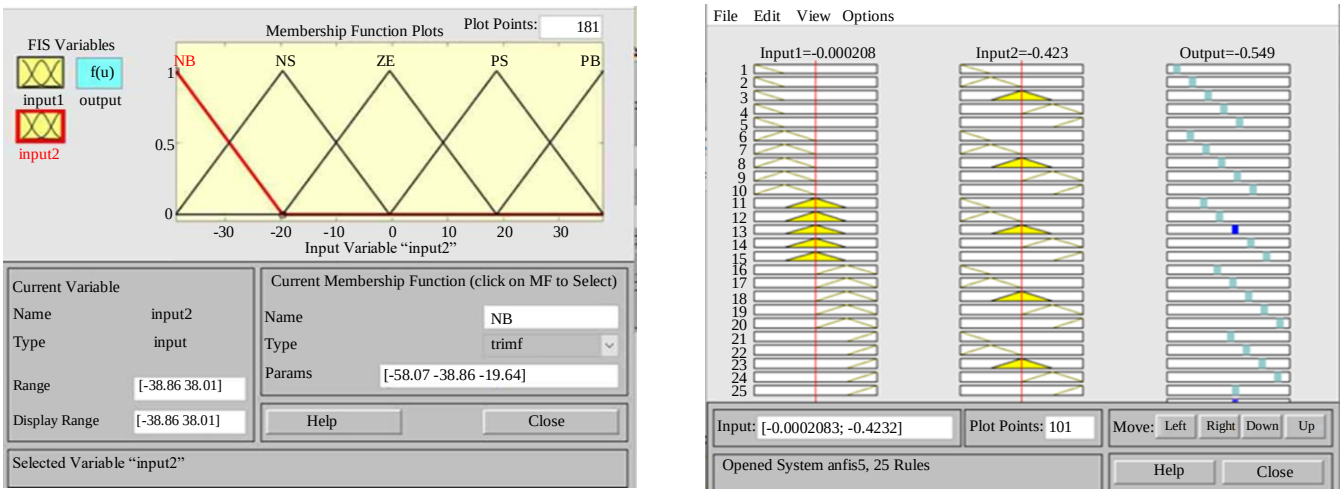

(c) (d)

Fig. 1 Inputs, output and fuzzy rules for FLC controller (a) Input1, (b) Input1, (c) Output 1, and (d) Input 2.

3.3. ANFIS Torque Controller Design

The ANFIS controller consists of five layers: input layer, input member function layer, rule layer, output member function layer, and output layer. The decision tree fuzzy interference involves categorizing data into linear regression models to minimize the total Squared Error (SSE) calculated by Equation 15.

The ANFIS controller uses a hybrid learning algorithm that combines the benefits of neural networks and fuzzy logic systems. By adjusting the parameters of the fuzzy inference system through backpropagation, the ANFIS controller can adapt and optimize its performance over time. This adaptive capability makes ANFIS controllers well-suited for applications with complex or unknown underlying system dynamics.

$$SSE \sum_i er_i^2 \tag{15}$$

Where n is the number of input variables, P denotes the fuzzy partition for each input variable, and er_i^2 is the discrepancy between the intended and actual output.

Figure 2 displays the Sugeno fuzzy model with two inputs. In this model, each input variable is fuzzified using a set of linguistic terms defined by the fuzzy partition P. The fuzzy rules are then applied to determine the output based on the values of the input variables.

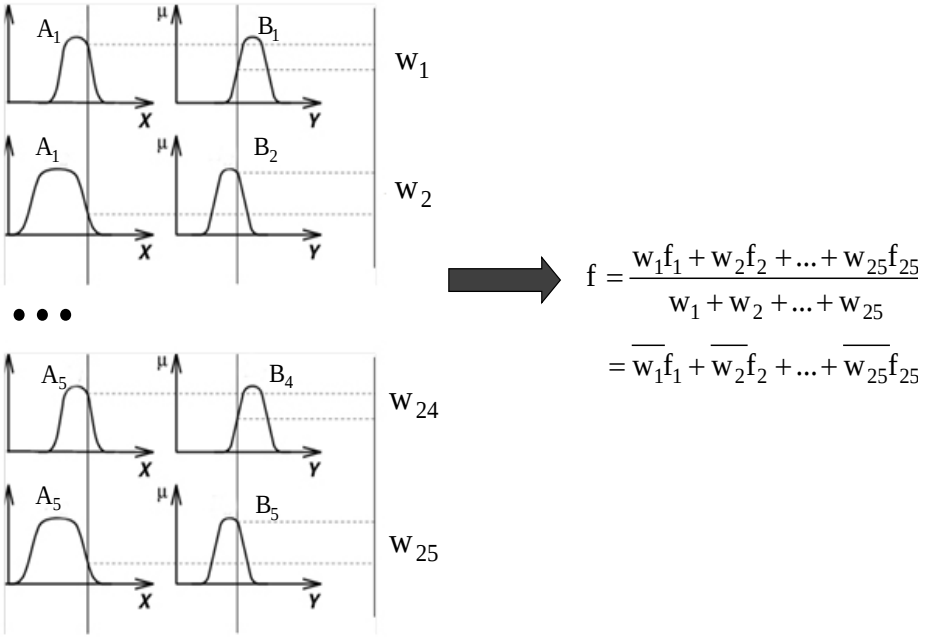

$$f = \frac{w_1 f_1 + w_2 f_2 + \ldots + w_{25} f_{25}}{w_1 + w_2 + \ldots + w_{25}} = \overline{w_1} f_1 + \overline{w_2} f_2 + \ldots + \overline{w_{25}} f_{25}$$

Fig. 2 The two-input Sugeno fuzzy logic control model

The ANFIS controller for current i_{sq} consists of two inputs: the difference (e) between i_{sq}* and i_{sq}, and error integral (Δe). The input signal is fuzzy into five triangular membership functions: Negative Big (NB), Negative Small (NS), Equal Zero (ZE), Positive Small (PS), and Positive Big (PB). The 5x5 = 25 fuzzy rules that combine with the output according to the two-input first-order Surgeon model:

- If x_1 is A_1 (NB) and x_2 is B1 (NB), then $f_1 = p1e + q_1\Delta e + r_1$If x_1 is A_1 (NB) and x_2 is B2 (NS), then $f_2 = p2e + q_2\Delta e + r_2$
- If x_1 is A_1 (NB) and x_2 is B3 (ZE), then $f_3 = p3e + q_3\Delta e + r_3$
- If x_1 is A_1 (NB) and x_2 is B3 (ZE), then $f_5 = p4e + q_4\Delta e + r_4$
- If x_1 is A_1 (NB) and x_2 is B3 (ZE), then $f_5 = p5e + q_5\Delta e + r_5$
- ……..
- If x_1 is A_{25} (PB) and x_2 is B_{25} (PB), then $f_{25} = p_{25}e + q_{25}\Delta e + r_{25}$

Where A_i and B_i are the premise fuzzy sets, and the parameters p_i, q_i, and r_i are the fuzzy design parameters calculated during the training process (i=1, 2,…n). The two-input and one-output NFC structure is given as follows:

The First Layer 1: The fuzzy process, takes place when the input signal is blurred into five triangular membership functions. For each output value of the first layer, we can quickly compute a membership function value denoted μ.

$$O_i^{layer1} = \mu_{Ai}(e) \quad (i = 1,2 \dots 5) \tag{16}$$

$$O_i^{layer1} = \mu_{Bi}(\Delta e) \quad (i = 1,2 \dots 5) \tag{17}$$

Where: i is the membership level of the dataset (A_1, A_2, B_1, B_2) and, $O_i^{layer\ 1}$ is the output of the i node in layer 1.

2nd layer is to check the weight of each function. This layer takes input values from the first layer and acts as optimization functions to represent data sets of corresponding input variables. The output of this node is described as follows:

$$O_1^{layer2} = w_1 = \mu_{A1}(e)\ x\ \mu_{B1}\ (\Delta e) \tag{18}$$

$$O_2^{layer2} = w_2 = \mu_{A2}(e)\ x\ \mu_{B2}\ (\Delta e) \tag{19}$$

……..

$$O_{25}^{layer2} = w_{25} = \mu_{A25}(e)\ x\ \mu_{B25}\ (\Delta e) \tag{20}$$

3rd Layer: This is a rule layer and takes input from the previous layer. Each node (each neuron) in this layer performs conditional matching of the rules. This layer calculates the activation level of each rule, and the number of layers is equivalent to the number of fuzzy rules. Each node of this class computes a weight that will be normalized. Layer 3 nodes calculate the ratio of the rule's activation strength to the sum of all active rules:

$$O_i^{layer3} = \overline{w_i} = \frac{w_i}{w_1+w_2+\cdots+w_{25}} \tag{21}$$

4th Layer: Defuzzification provides output values due to inference rules. The node output is calculated by multiplying the layer 3 output value and the corresponding rule:

$$O_i^{layer4} = \overline{w_i} = \frac{w_i}{w_1+w_2+\cdots+w_{25}}$$
(i=1,2, … 25) (22)

5th Layer: the output layer aggregates all inputs coming from the 4th layer and converts fuzzy classification results into the required value:

$$O_i^{layer5} = \sum_{i=1}^{25} \overline{w_i} f = \frac{w_1 f_1 + w_2 f_2 + \cdots + w_{25} f_{25}}{w_1+w_2+\cdots+w_{25}} \tag{23}$$
(i=1,2, … 25)

4. Simulation Results

4.1. Developing Paths for Electric Cars' Acceleration, Deceleration, and Operation Modes

The paths of acceleration and deceleration systems in electric vehicles are planned according to the equation y = F (x1, x2, …xn). Electric cars' accelerator and brake trajectories are determined by a function F, typically obtained through experimental derivation. The output is calculated by referencing or interpolating a table of values defined using block parameters, employing linear-gradient, Lagrange, nearest point, block spline, and Akima spline. The Fcos function typically ranges from 1 to 30 values. The first input defines dimension breakpoints for rows, while the second sets breakpoints for columns. This establishes the trajectories for the accelerator and brake systems in electric cars.

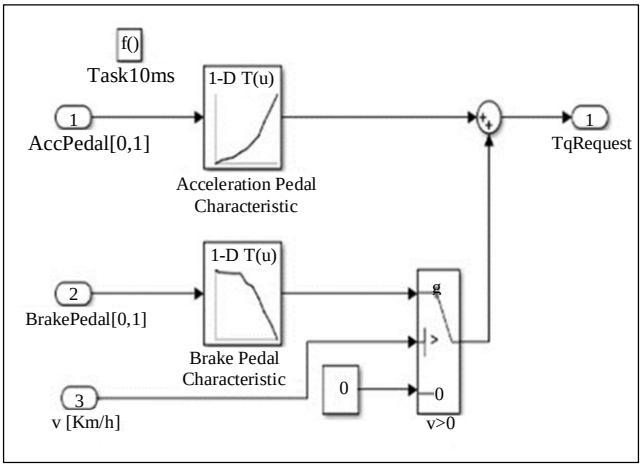

Fig. 3 The trajectories of the accelerator and brakes

Breakpoints	Column	(1)
Row		--
(1)	**0**	0
(2)	**0.1**	8.2
(3)	**0.2**	14.350000
(4)	**0.30000**	20.5
(5)	**0.4**	32.8
(6)	**0.5**	41
(7)	**0.6**	61.5
(8)	**0.7**	82
(9)	**0.8**	123
(10)	**0.9**	164
(11)	**1**	205

(a)

Breakpoints	Column	(1)
Row		--
(1)	**0**	0
(2)	**0.03**	0
(3)	**0.04**	-8.2
(4)	**0.3**	-10.25
(5)	**0.4**	-12.2999
(6)	**0.5**	-41
(7)	**0.6**	-51.25
(8)	**0.7**	-82
(9)	**0.8**	-123
(10)	**0.9**	-164
(11)	**1**	-205

(b)

Fig. 4 The parameters trajectories of the accelerator and brakes

4.2. Simulation Results for PI, FLC and ANFIS Torque Controllers

Figure 5 illustrates the control structure of the traction drive system for electric vehicles utilizing the in-wheel AFPMSM motor.

Table 2 lists the simulation parameters. Evaluating the controller's efficiency for the traction transmission system in electric cars employing an in-wheel AFPMSM motor entails running simulations in MATLAB under specific conditions.

- Wind speed is assumed to be 0.
- The vehicle moves on a flat surface but descends between t = 3.5s and t = 4.3s.
- Acceleration of the vehicle begins at t = 0s, with the accelerator value rising from 0 to 1 after 0.45s. The torque reaches a peak of 205 Nm and remains constant for 2 seconds.
- The torque gradually decreases to -205 Nm, returning to 0 at t = 4.66s.

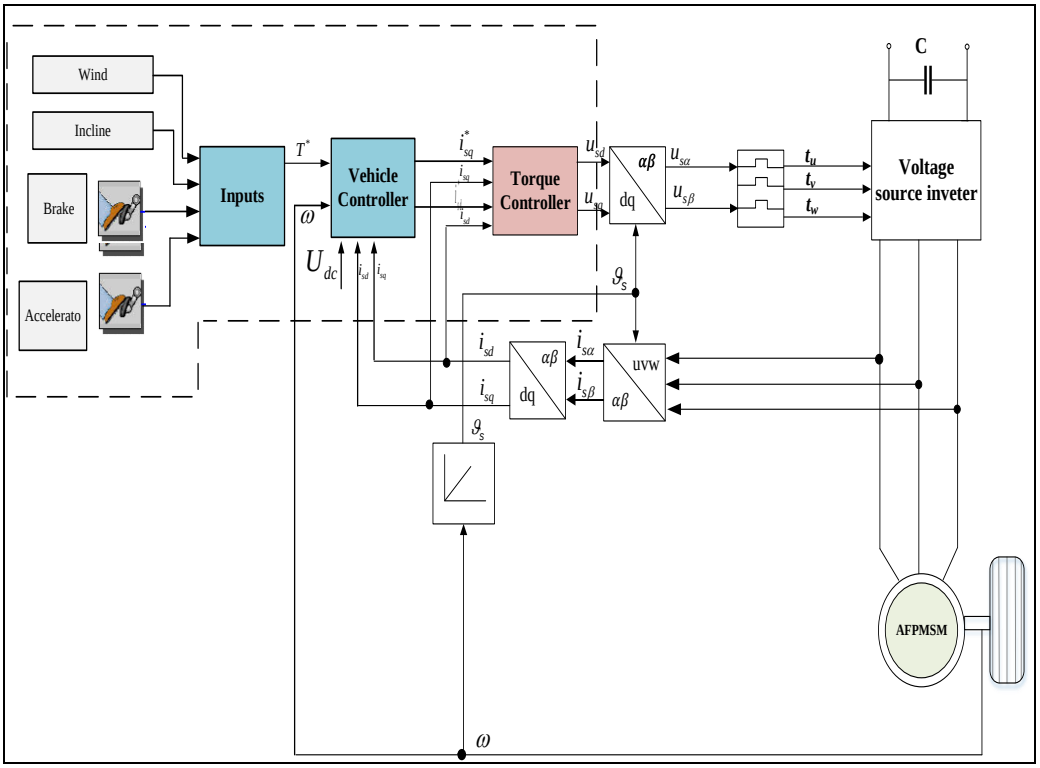

Fig. 5 The control structure for electric cars using an AFPMSM motor-based FOC control method

The PI controller is established using a specific set of integral and gain parameters, outlined in Table 2. Comparisons of stator current responses between the FLC, ANFIS torque controller, and PI controller are depicted in Figures 6, 7, and 8. Table 2 presents the stator's current PI, FLC, and ANFIS controller responsiveness evaluation criteria. The comparative analysis of stator current responses across the three controllers reveals varying degrees of performance in managing stator current variations. With its integral parameter set to 0.1 and gain parameter set to 0.05, the PI controller demonstrates a certain level of responsiveness in regulating the stator current.

Table 2. Parameters for an AFPMSM motor

Controller	K_i	K_p
Stator Current Controller i_{sd}	7.103004e+2	0.8779
Stator Current Controller i_{sq}	1.0615e+3	1.0744

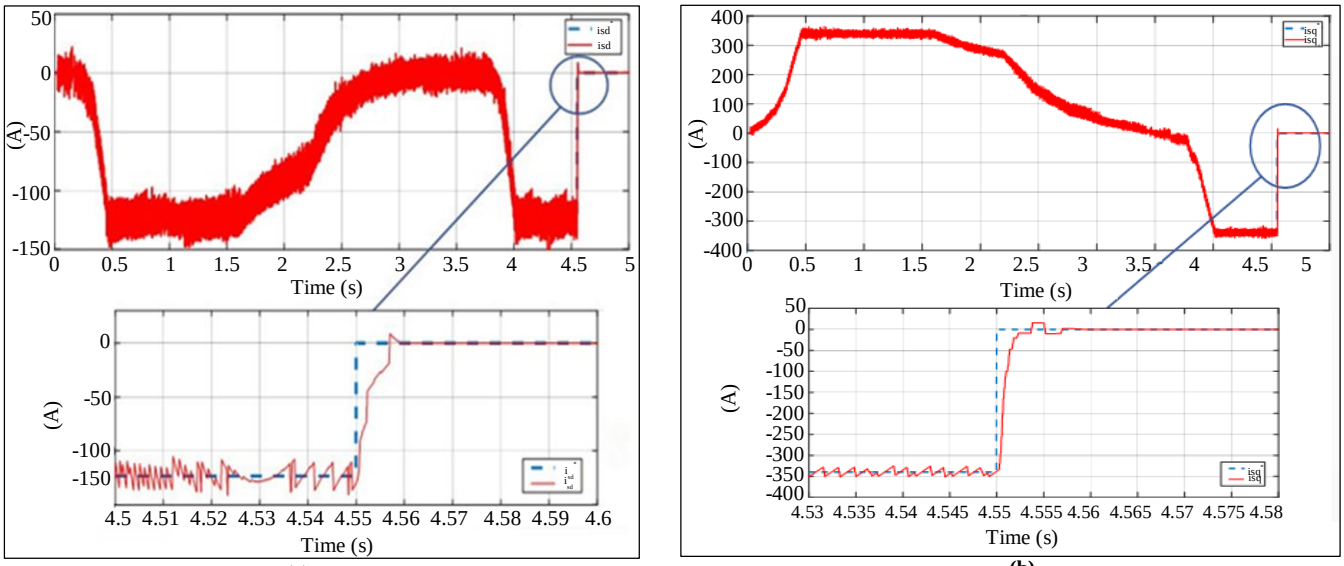

(a) **(b)**

Fig. 6 Current stator responses of PI controller (a) Current response i_{sd}, and (b) Current response i_{sq}.

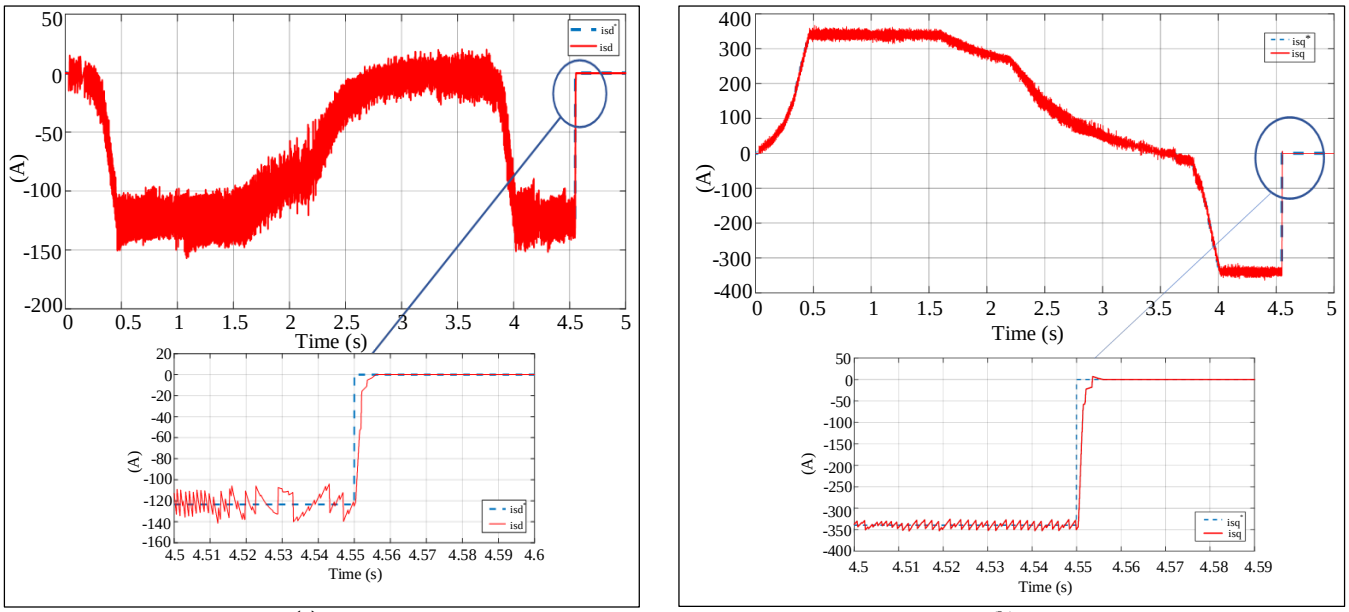

(a) **(b)**

Fig. 7 Current stator responses of FLC controller (a) Current response i_{sd}, and (b) Current response i_{sq}.

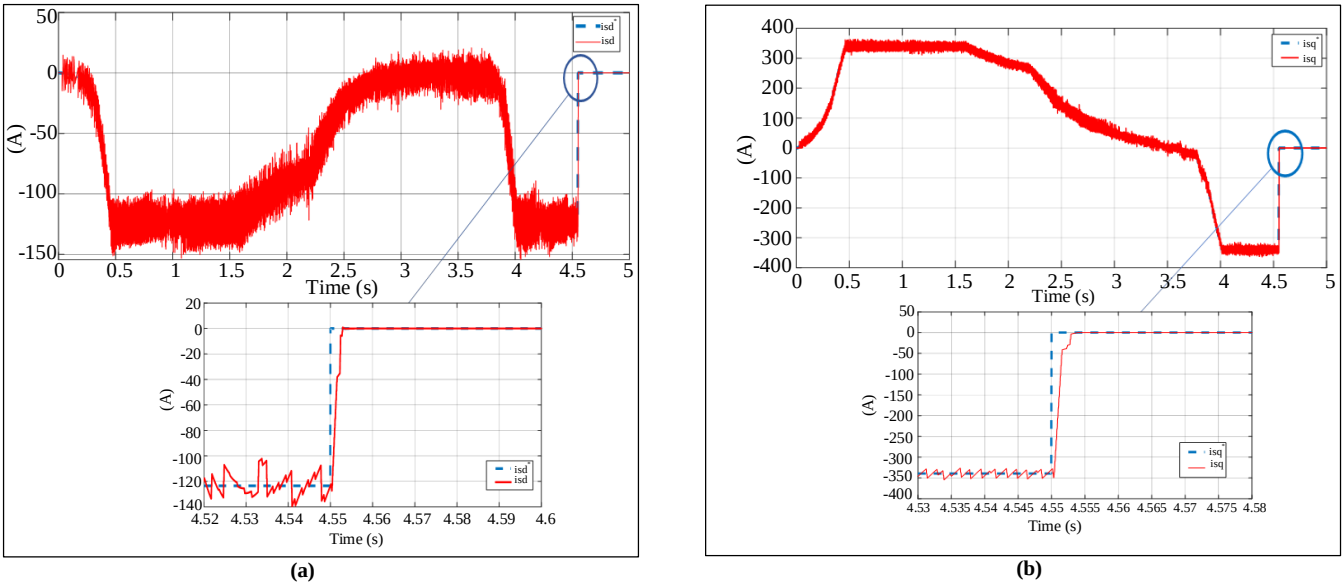

(a) (b)

Fig. 8 Current stator responses of ANFIS controller (a) Current response i_{sd}, and (b) Current response i_{sq}.

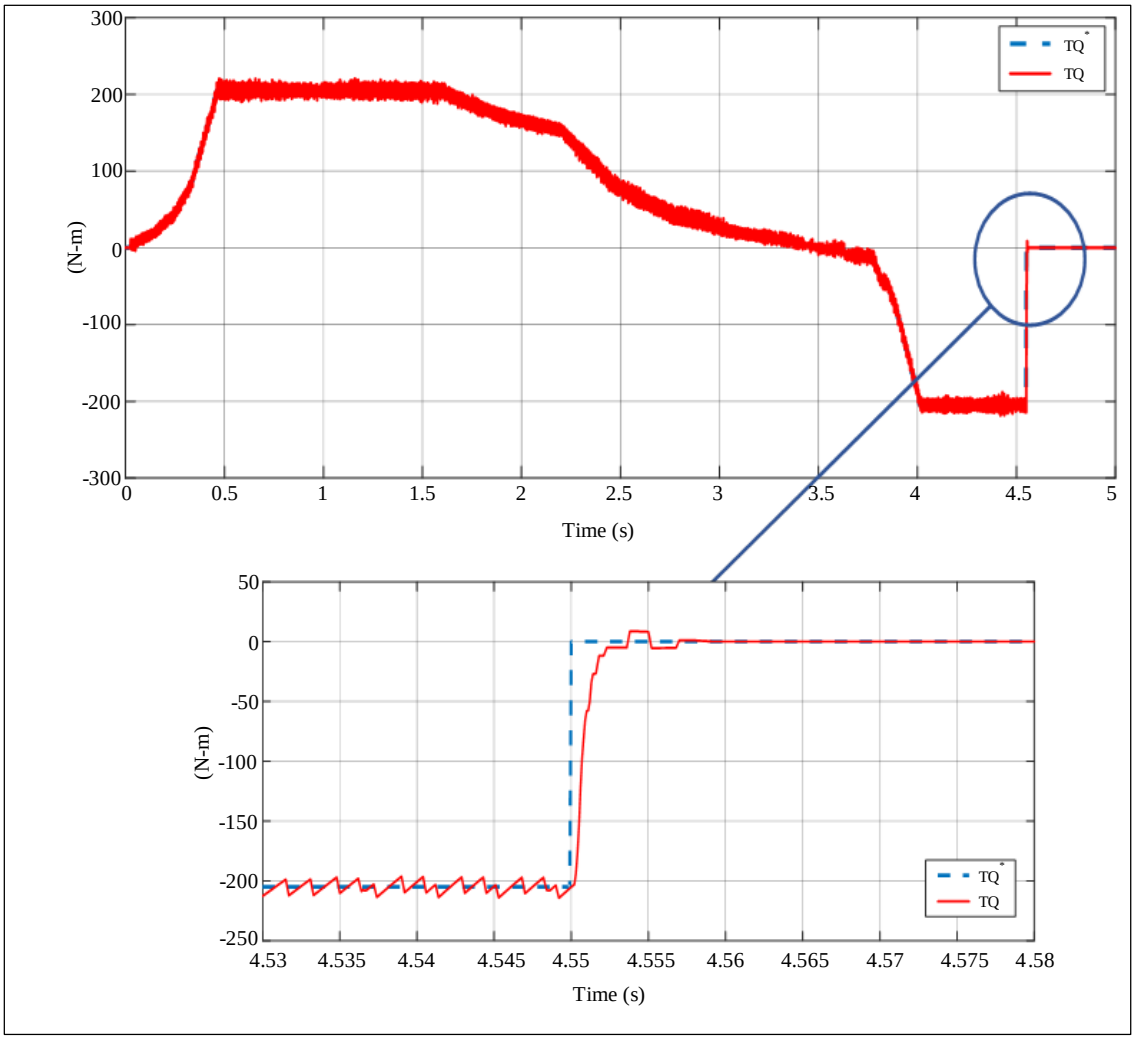

Fig. 9 The torque response of PI controller

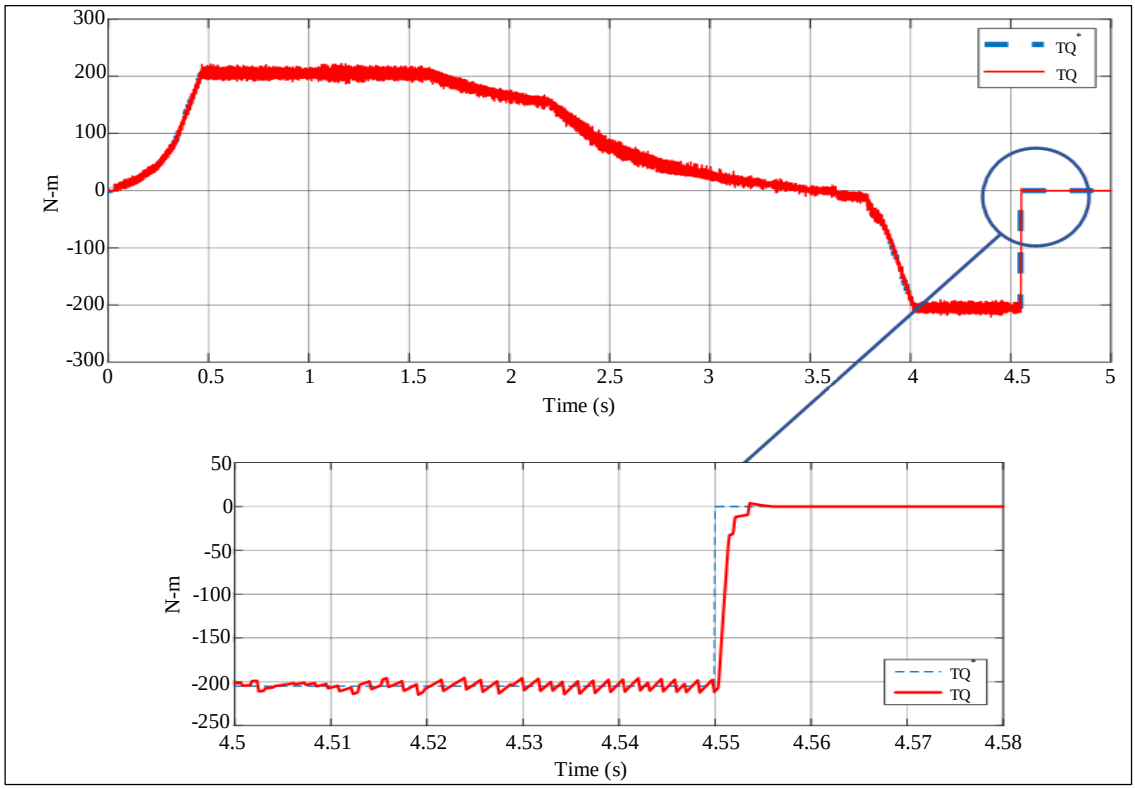

Fig. 10 The torque response of FLC controller

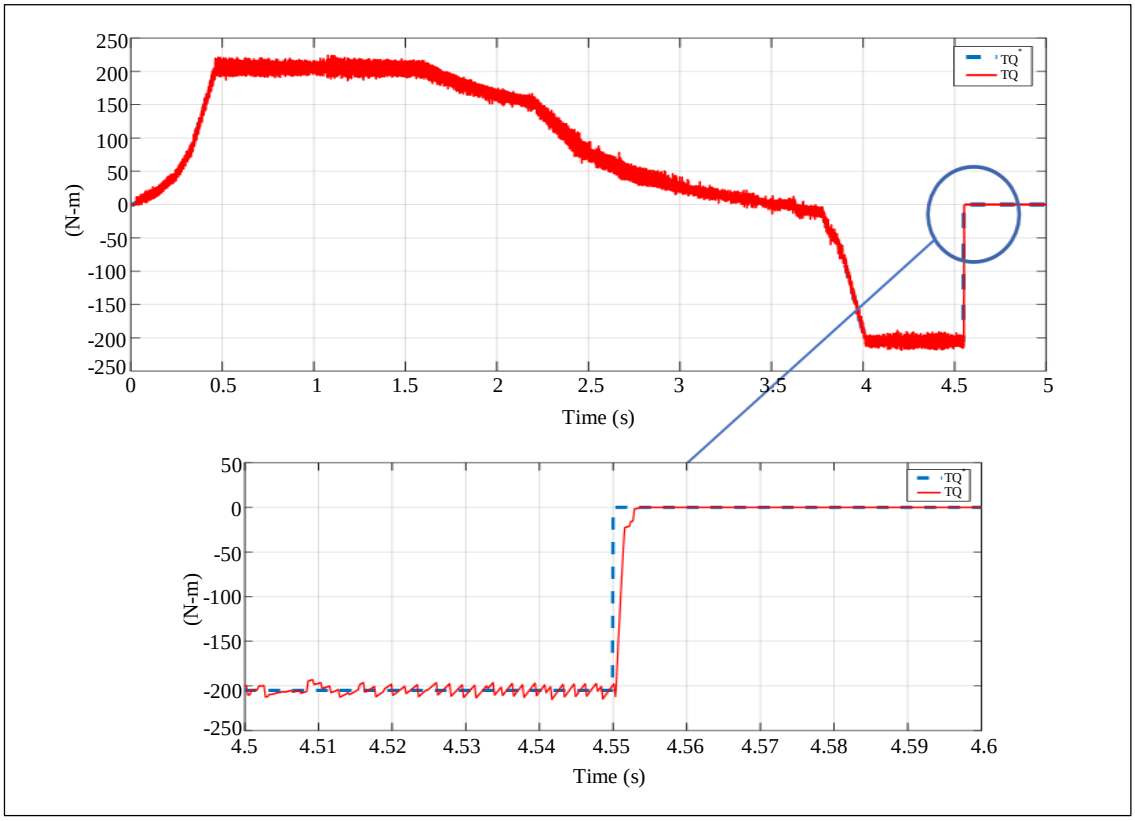

Fig. 11 The torque response of ANFIS controller

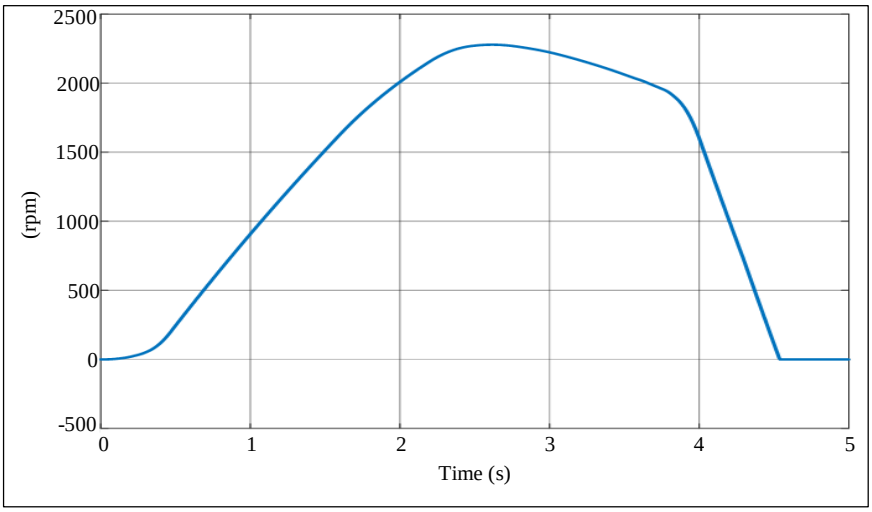

Fig. 12 Speedy responses for PI and FLC controller

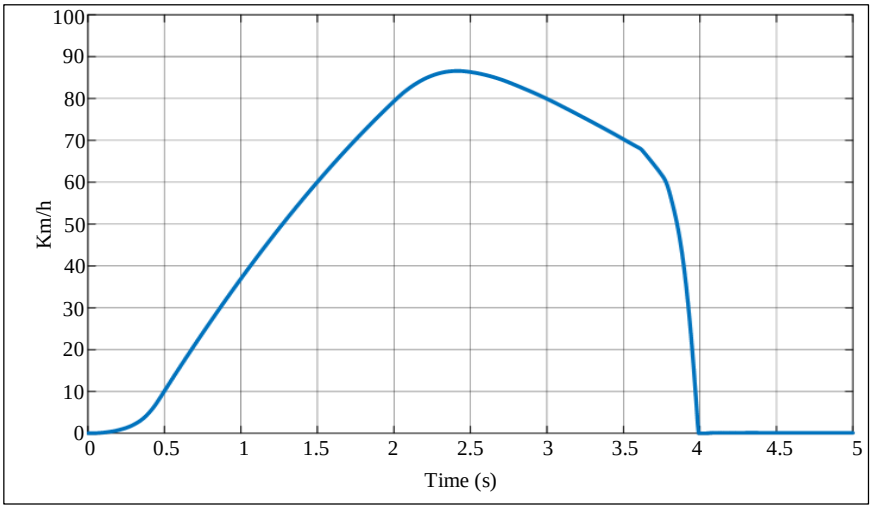

Fig. 13 The speed response of ANFIS controller

Table 3. Results of evaluation responsibility

Controller/Parameter Evaluation PI	PI	FLC	ANFIS
Torque Responses			
Torque Fluctuation	Same as i_{sq} Current Response	Same as i_{sq} Current Response	Same as i_{sq} Current Response
The Torque Ripple	8%	5%	3%
Speedy Responses			
Quickened Curing Period	2.2 (s)	2.2 (s)	2.2 (s)
Overcorrection	0%	0%	0%

Figures 9, 10, and 11 demonstrate that the torque of the three controllers follows the same pattern as the isq stator current. The ANFIS controller has a higher torque response than the other controller, with a difference of 3%. On the other hand, FLC controllers for torque ripple response have a lower pulse rate (5%) than the PI controller (8%). Furthermore, the electric car's speed response from both controllers meets the specified parameters without excessive speed adjustments. Additionally, the efficiency analysis reveals that the ANFIS controller outperforms the other controllers by achieving a 7% increase in overall efficiency. The FLC controllers also show promising results in terms of efficiency, with a 4%

improvement compared to the PI controller. This demonstrates the effectiveness of advanced control strategies in enhancing the performance of electric vehicles.

The comparative study highlights the potential for further advancements in controller design to optimize the operation of electric propulsion systems. The speed response of the electric automobile from both controllers meets the stated parameters without excessive speed adjustments while beginning, accelerating, and decelerating, as shown in Figures 12 and 13.

5. Conclusion

The research successfully designed an in-wheel AFPMSM motor torque controller for a traction drive system using an FLC and NFC controller by MATLAB simulation. Two controllers are compared with the PI controller. Simulation results show that the torque response of the FLC and NFC controllers is fast and follows the set value, while the PI controller has a slower response and high throttling transients. The resulting torque amplitude is also smaller with the NFC controller compared to the PI and FLC control methods. The stability of the PI controller is destabilized when the motor parameter changes, while the FLC and NFC controllers provide better system stability.

However, these FLC and NFC controllers have a complicated design, so studying simple, intelligent control solutions in theoretical implementation and experimental performance in the future is necessary. Developing simple, intelligent control solutions is crucial for the practical implementation and experimental performance of the in-wheel AFPMSM motor torque controller. By focusing on theoretical advancements and real-world testing, researchers can refine and optimize the control methods to ensure efficient and reliable operation in traction drive systems. This approach will simplify the design process and enhance the overall stability and performance of the motor torque controller, ultimately leading to more effective and practical implementation in various applications.

Acknowledgements

This research is funded by the University of Transport and Communications (UTC) under grant number T2023-DT-001 TĐ.

References

[1] Xudong Zhang, Dietmar Göhlich, and Jiayuan Li, "Energy-Efficient Toque Allocation Design of Traction and Regenerative Braking for Distributed Drive Electric Vehicles," *IEEE Transactions on Vehicular Technology*, vol. 67, no. 1, pp. 285-295, 2018. [CrossRef] [Google Scholar] [Publisher Link]

[2] Nobuyoshi Mutoh, "Driving and Braking Torque Distribution Methods for Front- and Rear-Wheel-Independent Drive-Type Electric Vehicles on Roads with Low Friction Coefficient," *IEEE Transactions on Industrial Electronics*, vol. 59, no. 10, pp. 3919-3933, 2012. [CrossRef] [Google Scholar] [Publisher Link]

[3] X. Yuan, J. Wang, and K. Colombage, "Torque Distribution Strategy for a Front and Rear-Wheel-Driven Electric Vehicle," *IEEE Transactions on Vehicular Technology*, vol. 61, no. 8, pp. 3365-3374, 2012. [CrossRef] [Google Scholar] [Publisher Link]

[4] Rafal Wrobel et al., "Design Considerations of a Brushless Open-Slot Radial-Flux PM Hub Motor," *IEEE Transactions on Industry Applications*, vol. 50, no. 3, pp. 1757-1767, 2014. [CrossRef] [Google Scholar] [Publisher Link]

[5] Wei Xu et al., "Survey on Electrical Machines in Electrical Vehicles," *2009 International Conference on Applied Superconductivity and Electromagnetic Devices*, Chengdu, China, pp. 167-170, 2009. [CrossRef] [Google Scholar] [Publisher Link]

[6] Mohamed Arbi Khlifi et al., "Investigation of a Leakage Reactance Brushless DC Motor for DC Air Conditioning Compressor," *Engineering Technology & Applied Science Research*, vol. 12, no. 2, pp. 8316-8320, 2022. [CrossRef] [Google Scholar] [Publisher Link]

[7] Merve Yildirim, Mehmet Polat, and Hasan Kürüm, "A Survey on Comparison of Electric Motor Types and Drives Used for Electric Vehicles," *2014 16th International Power Electronics and Motion Control Conference and Exposition*, Antalya, Turkey, pp. 218-223, 2014. [CrossRef] [Google Scholar] [Publisher Link]

[8] Tahir Aja Zarma, Ahmadu Adamu Galadima, and Aminu A. Maruf, "Review of Motors for Electrical Vehicles," *Journal of Scientific Research and Reports*, vol. 24, no. 6, pp. 1-6, 2019. [CrossRef] [Google Scholar] [Publisher Link]

[9] Xavier del Toro Garcia et al., "Comparison between FOC and DTC Strategies for Permanent Magnet Synchronous Motors," *Advances in Electrical and Electronic Engineering*, vol. 5, no. 1, pp. 76-81, 2011. [Google Scholar] [Publisher Link]

[10] Pooja Bhatt, Hemant Mehar, and Manish Sahajwani, "Electrical Motors for Electric Vehicle-A Comparative Study," *Proceedings of Recent Advances in Interdisciplinary Trends in Engineering & Applications (RAITEA)*, pp. 1-10, 2019. [CrossRef] [Google Scholar] [Publisher Link]

[11] Weiguang Yu, and Chenglin Gu, "Dynamic Analysis of a Novel Clutch System for In-Wheel Motor Drive Electric Vehicles," *IET Electric Power Applications*, vol. 11, no. 1, pp. 90-98, 2017. [CrossRef] [Google Scholar] [Publisher Link]

[12] Araz Darba, Mohammad Esmalifalak, and Ebrahim Sarbaz Barazandeh, "Implementing SVPWM Technique to Axial Flux Permanent Magnet Synchronous Motor Drive with Internal Model Current Controller," *2010 4th International Power Engineering and Optimization Conference (PEOCO)*, Shah Alam, Malaysia, pp. 126-131, 2010. [CrossRef] [Google Scholar] [Publisher Link]

[13] Ramu Krishnan, *Electric Motor Drives: Modeling, Analysis, and Control*, Prentice-Hall of India Pvt. Limited, 2001. [Google Scholar] [Publisher Link]

[14] Chunyu Yang, Leping Shen, and Linna Zhou, "Fuzzy Sliding Mode Control for Permanent Magnet Synchronous Motors," *2018 5th International Conference on Information, Cybernetics, and Computational Social Systems (ICCSS)*, Hangzhou, China, pp. 331-336, 2018. [CrossRef] [Google Scholar] [Publisher Link]

[15] Trong Duy Nguyen et al., "A Novel Axial Flux Permanent-Magnet Machine for Flywheel Energy Storage System: Design and Analysis," *IEEE Transactions on Industrial Electronics*, vol. 58, no. 9, pp. 3784-3794, 2011. [CrossRef] [Google Scholar] [Publisher Link]

[16] Trong Duy Nguyen et al., "Modeling and Position-Sensorless Control of a Dual-Airgap Axial Flux Permanent Magnet Machine for Flywheel Energy Storage Systems," *Journal of Power Electronics*, vol. 12, no. 5, pp. 758-768, 2012. [CrossRef] [Google Scholar] [Publisher Link]

[17] S. Nakashima, Y. Inagaki, and I. Miki, "Sensorless Initial Rotor Position Estimation of Surface Permanent-Magnet Synchronous Motors," *IEEE Transactions on Industry Applications*, vol. 36, no. 6, pp. 1598-1603, 2000. [CrossRef] [Google Scholar] [Publisher Link]

[18] Freescale, Sensorless PMSM Vector Control, Design Reference Manual, pp. 1-62, 2009. [Online]. Available: https://www.nxp.com/docs/en/reference-manual/DRM109.pdf

[19] V.K. Arun Shankar et al., "Adaptive Neuro-Fuzzy Inference System (ANFIS) Based Direct Torque Control of PMSM Driven Centrifugal Pump," *International Journal of Renewable Energy Research*, vol. 7, no. 3, pp. 1437-1447, 2017. [Google Scholar] [Publisher Link]

[20] Dmitry V. Lukichev et al., "Application of Adaptive Neuro Fuzzy Inference System (ANFIS) Controller in Servodrive with Multi-Mass Object," *2018 25th International Workshop on Electric Drives: Optimization in Control of Electric Drives (IWED)*, Moscow, Russia, pp. 1-6, 2018. [CrossRef] [Google Scholar] [Publisher Link]

[21] Nagham Farhan, Abdulrahim T. Humod, and Fadhil A. Hasan, "Field Oriented Control of AFPMSM for Electrical Vehicle Using Adaptive Neuro-Fuzzy Inference System (ANFIS)," *Engineering Engineering and Technology Journal*, vol. 39, no. 10, pp. 1571-1582, 2021. [CrossRef] [Google Scholar] [Publisher Link]